

Drawing conformal diagrams for a fractal landscape

Sergei Winitzki

Department of Physics, Ludwig-Maximilians University, Theresienstr. 37, 80333 Munich, Germany

Generic models of cosmological inflation and the recently proposed scenarios of a recycling universe and the string theory landscape predict spacetimes whose global geometry is a stochastic, self-similar fractal. To visualize the complicated causal structure of such a universe, one usually draws a conformal (Carter-Penrose) diagram. I develop a new method for drawing conformal diagrams, applicable to arbitrary 1+1-dimensional spacetimes. This method is based on a qualitative analysis of intersecting lightrays and thus avoids the need for explicit transformations of the spacetime metric. To demonstrate the power and simplicity of this method, I present derivations of diagrams for spacetimes of varying complication. I then apply the lightray method to three different models of an eternally inflating universe (scalar-field inflation, recycling universe, and string theory landscape) involving the nucleation of nested asymptotically flat, de Sitter and/or anti-de Sitter bubbles. I show that the resulting diagrams contain a characteristic fractal arrangement of lines.

I. INTRODUCTION

Generic models of cosmological inflation predict that thermalization will never be reached everywhere in the universe. This phenomenon, termed *eternal inflation*, was first analyzed for scalar-field inflationary scenarios [1, 2]. The resulting spacetime is inhomogeneous since some regions will still undergo inflation while other regions have thermalized. Inhomogeneities of this type occur at distances much larger than the Hubble scale H^{-1} . With eternal inflation, the proper volume of the non-thermalized (inflating) domain grows with time and forms a self-similar lacunary fractal, first studied in Ref. [3]. An increasing number of regions thermalize at progressively later times (this statement is independent of the choice of an equal-time slicing), and moreover it can be shown that there exist infinitely many comoving geodesics that never enter any thermalized regions [4].

Besides scalar field-driven inflation, there exist other cosmological scenarios with a similar stochastic and fractal geometry of the spacetime. These are for instance the models of a *recycling universe* [5] and the *string theory landscape* [6]. In these scenarios, various de Sitter (or anti-de Sitter) regions can nucleate as bubbles within the background de Sitter spacetime and within other bubbles. It is an interesting challenge to visualize the causal structure of such a spacetime. In particular, the geometry of an asymptotic future infinity is relevant to considerations of the holographic principle [7, 8, 9].

The purpose of this paper is to construct conformal diagrams (also called *Carter-Penrose diagrams*) for spacetimes arising from models of eternal inflation. All such spacetimes consist of approximately homogeneous Hubble-size regions expanding at different rates and forming a fractal structure on super-Hubble scales. I describe a new method of drawing conformal diagrams for spacetimes where the metric cannot be obtained in closed form. This method is based on a qualitative analysis of the asymptotic behavior of lightrays in the given spacetime and does not require deriving explicit conformal transformations of the metric. I illustrate the

new method on some standard as well as novel examples. I then apply this method to construct conformal diagrams for various models of an eternally inflating universe. The models of interest are: a generic inflation producing either matter-dominated or dark energy-dominated domains; a recycling universe that generates a never-ending sequence of nested thermalized and inflating (de Sitter) domains; and the string theory landscape which includes recycling and also admits anti-de Sitter bubbles ending in a singularity. I show that conformal diagrams representing the resulting spacetimes can be drawn using a random fractal arrangement of lines. I present computer-simulated conformal diagrams that help visualize the causal structure of such spacetimes. In particular, it becomes apparent that these spacetimes possess an infinite number of points representing different causally disconnected null and timelike conformal infinities.

II. DRAWING CONFORMAL DIAGRAMS

After recapitulating the standard construction of conformal diagrams, I shall develop a new, easier method that will be used throughout the paper.

A. Standard procedure

A conformal diagram is defined for a 1+1-dimensional spacetime with a given line element $g_{ab}dx^a dx^b$. The coordinates x^a (where $a = 0, 1$) must cover the entire spacetime, and several sets of overlapping coordinate patches may be used if necessary. The standard construction of the conformal diagram may be formulated as follows (see e.g. [10], chapter 3). One first finds a change of coordinates $x \rightarrow \tilde{x}$ such that the new variables \tilde{x}^a have a *finite* range of variation; the components of the metric change according to $g_{ab}(x)dx^a dx^b = \tilde{g}_{ab}(\tilde{x})d\tilde{x}^a d\tilde{x}^b$. One then chooses a conformal transformation of the metric (in the

new coordinates),

$$\tilde{g}_{ab} \rightarrow \gamma_{ab}(\tilde{x}) = \Omega^2(\tilde{x}) \tilde{g}_{ab}, \quad \Omega(\tilde{x}) \neq 0, \quad (1)$$

such that the new metric γ_{ab} is flat, i.e. has zero curvature. A suitable function $\Omega(\tilde{x})$ always exists because all two-dimensional metrics are conformally flat. The new metric γ_{ab} describes an unphysical, auxiliary flat spacetime. Since the metric γ_{ab} is flat, a further change of coordinates $\tilde{x} \rightarrow \tilde{\tilde{x}}$ (the new variables $\tilde{\tilde{x}}$ again having a finite extent) can be found to transform γ_{ab} explicitly into the Minkowski metric η_{ab} ,

$$\gamma_{ab}(\tilde{x}) d\tilde{x}^a d\tilde{x}^b = \eta_{ab} d\tilde{\tilde{x}}^a d\tilde{\tilde{x}}^b, \quad \eta_{ab} \equiv \text{diag}(1, -1). \quad (2)$$

For brevity we incorporate all the required coordinate changes into one, $x \rightarrow \tilde{x}(x)$, and summarize the transformation of the metric as

$$\Omega^2(x) g_{ab} dx^a dx^b = \eta_{ab} d\tilde{x}^a d\tilde{x}^b. \quad (3)$$

Thus the new coordinates \tilde{x}^a map the initial spacetime onto a *finite* domain within a 1+1-dimensional Minkowski plane. This finite domain is a *conformal diagram* of the initial (physical) 1+1-dimensional spacetime. The diagram is drawn on a sheet of paper which implicitly carries the fiducial Minkowski metric η_{ab} , the vertical axis usually representing the timelike coordinate \tilde{x}^0 .

The coordinate and conformal transformations severely distort the geometry of the spacetime since they bring infinite spacetime points to finite distances in the diagram plane. So one cannot expect in general that straight lines in the diagram correspond to geodesics in the physical spacetime. However, it is well-known that straight lines drawn at 45° angles in a conformal diagram represent null geodesics in the physical spacetime. This follows from the fact that any null trajectory $x^a(\tau)$ in 1+1 dimensions, i.e. any solution of

$$g_{ab} \dot{x}^a \dot{x}^b = 0, \quad \dot{x}^a \equiv \frac{dx^a}{d\tau}, \quad (4)$$

is necessarily a geodesic (this is not true in higher dimensions), and Eq. (4) is invariant under conformal transformations of the metric. By drawing lightrays emitted from various points in the diagram, one can illustrate the causal structure of the spacetime.

A textbook example is the conformal diagram for the flat Minkowski spacetime with the metric $g_{ab} \equiv \eta_{ab}$. Calculations are conveniently done in the lightcone coordinates

$$u \equiv x^0 - x^1, \quad v \equiv x^0 + x^1, \quad \eta_{ab} dx^a dx^b = du dv, \quad (5)$$

and a suitable coordinate transformation is

$$\tilde{u} = \tanh u, \quad \tilde{v} = \tanh v, \quad du dv = \frac{d\tilde{u} d\tilde{v}}{(1 - \tilde{u}^2)(1 - \tilde{v}^2)}. \quad (6)$$

The new coordinates \tilde{u}, \tilde{v} extend from -1 to 1 . Multiplying the metric by the conformal factor $\Omega^2(\tilde{u}, \tilde{v}) \equiv$

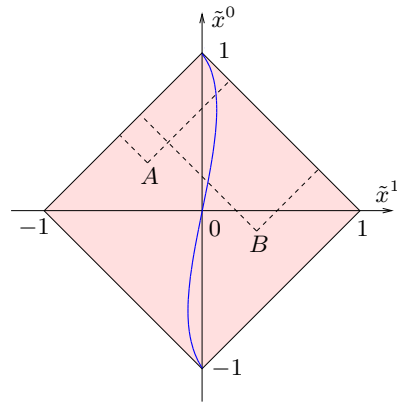


Figure 1: A conformal diagram of the 1+1-dimensional Minkowski spacetime. Dashed lines show lightrays emitted from points A, B . The curved line is the trajectory of an inertial observer moving with a constant velocity, $x^1 = 0.3x^0$.

$(1 - \tilde{u}^2)(1 - \tilde{v}^2)$, we obtain the fiducial spacetime,

$$\Omega^2 du dv = d\tilde{u} d\tilde{v} = \eta_{ab} d\tilde{x}^a d\tilde{x}^b, \quad (7)$$

$$\tilde{u} \equiv \tilde{x}^0 - \tilde{x}^1, \quad \tilde{v} \equiv \tilde{x}^0 + \tilde{x}^1. \quad (8)$$

The new coordinates \tilde{x}^a have a finite extent, namely $|\tilde{x}^0 \pm \tilde{x}^1| < 1$, and the resulting diagram has a diamond shape shown in Fig. 1. To appreciate the distortion of the spacetime geometry, we can draw the worldline of an inertial observer moving with a constant velocity. Note that the angle at which this trajectory enters the end-points depends on the chosen conformal transformation and thus cannot serve as an indication of the observer's velocity.

There is no analog of conformal diagrams for general 3+1-dimensional spacetimes. Nevertheless, in many cases a 3+1-dimensional spacetime can be adequately represented by a suitable 1+1-dimensional slice, at least for the purpose of qualitative illustration. For instance, a spherically symmetric spacetime is visualized as the (t, r) half-plane ($r \geq 0$) where each point stands for a 2-sphere of radius r . A conformal diagram is then drawn for the reduced 1+1-dimensional spacetime.

The reduced conformal diagram is meaningful only if the null geodesics in the 1+1-dimensional section are also geodesics in the physical 3+1-dimensional spacetime. In this case, the 1+1-dimensional section can be visualized as the set of events accessible to an observer who sends and receives signals only along a fixed spatial direction. Then a conformal diagram provides information about the causal structure of spacetime along this line of sight.

B. Method of lightrays

The standard construction of conformal diagrams involves an explicit transformation of the metric to new

coordinates that have a finite extent, and usually a further transformation to bring the metric to a manifestly conformally flat form. Finding these transformations requires a certain ingenuity. If the spacetime manifold is covered by several coordinate patches, a different transformation must be used in each patch. However, a conformal diagram typically consists of just a few lines and one would expect that the required computations should not be so cumbersome.

I now describe a method of drawing conformal diagrams that avoids the need for performing explicit transformations of the metric. The method is based on a qualitative analysis of intersections of lightrays. This approach is particularly suitable for the analysis of stochastic spacetimes encountered in models of eternal inflation. Such spacetimes have no symmetries and their metric is not known in closed form, so one cannot apply the standard construction of conformal diagrams.

Another motivation for the new method is the apparent redundancy involved in the standard method. It is clear that the transformations used in the standard construction are not unique. For instance, one may replace the lightcone coordinates in Eq. (6) by

$$\tilde{u} \rightarrow f(\tilde{u}), \quad \tilde{v} \rightarrow g(\tilde{v}), \quad (9)$$

where f, g are arbitrary monotonic, bounded, and continuous functions. The shape of the diagram will vary with each possible choice of the transformations, but all resulting diagrams are equivalent in the sense that they contain the same information about the causal structure of the spacetime. One thus expects to be able to extract this information without involving specific explicit transformations of the coordinates and the metric.

The crucial observation is that this information is unambiguously represented by the geometry and topology of lightrays and their intersections. I shall now develop this idea into a self-contained approach to drawing conformal diagrams that does not involve explicit transformations.

1. New definition of conformal diagrams

A conformal diagram is a figure in the fiducial Minkowski plane satisfying certain conditions, and I first formulate a definition of a conformal diagram in terms of such conditions. A constructive procedure for drawing conformal diagrams will be presented subsequently.

A finite open domain of the plane is a *conformal diagram* of a given 1+1-dimensional spacetime S if there exists a one-to-one correspondence between all maximally extended lightrays in S and all straight line segments drawn at 45° angles within the domain of the diagram. This correspondence must be *intersection-preserving*, i.e. any two lightrays intersect in the physical spacetime exactly as many times as the corresponding lines intersect in the diagram. It is assumed that all null geodesics in the spacetime S are either infinitely

extendible or end at singularities or at explicitly introduced spacetime boundaries. Similarly, the straight line segments drawn at 45° angles in a conformal diagram must be limited only by the boundary of the diagram. Note that there are only two spatial directions in a 1+1-dimensional spacetime S , and that two lightrays emitted in the same direction cannot intersect.

For example, the diamond $|\tilde{x}^0 \pm \tilde{x}^1| < 1$ is a conformal diagram for the flat spacetime due to the intersection-preserving one-to-one correspondence of null lines $\tilde{x}^0 \pm \tilde{x}^1 = \text{const}$ in the diagram and lightrays $x^0 \pm x^1 = \text{const}$ in the physical spacetime.

For spacetimes having a nontrivial topology, appropriate topological features need to be introduced also into the fiducial Minkowski plane. At this point I do not consider such cases.

I shall now demonstrate the equivalence of the proposed definition to the standard procedure for drawing conformal diagrams. It suffices to find a conformal transformation of the form (3) in some neighborhood of an arbitrary (nonsingular) spacetime point. Given a diagram with an intersection-preserving correspondence of lightrays, we can introduce local lightcone coordinates u, v in the diagram such that the null geodesics are locally the lines $u = \text{const}$ or $v = \text{const}$. By assumption, each null geodesic uniquely corresponds to a lightray in the physical spacetime. Since the correspondence is intersection-preserving, the local configuration of the null geodesics in the physical spacetime can be visualized as in Fig. 2. Hence the local lightcone coordinates u, v become well-defined local coordinates in the physical spacetime, and again the null geodesics are the lines $u = \text{const}$ or $v = \text{const}$. On the other hand, these null geodesics must be solutions of Eq. (4), therefore

$$g_{uu}\dot{u}^2 + 2g_{uv}\dot{u}\dot{v} + g_{vv}\dot{v}^2 = 0 \text{ if } \dot{u} = 0 \text{ or } \dot{v} = 0. \quad (10)$$

It follows that $g_{uu} = g_{vv} = 0$. Thus the metric in the local lightcone coordinates is of the form $g_{ab}dx^a dx^b = 2g_{uv}(u, v)du dv$ which is explicitly conformally flat. This demonstrates the existence of a local conformal transformation bringing the physical metric g_{ab} into the fiducial Minkowski metric $du dv = \eta_{ab}d\tilde{x}^a d\tilde{x}^b$ in the diagram.

Before presenting examples, I comment on the proposed definition of conformal diagrams. The definition may appear to be too broad, allowing many geometric shapes to represent the same spacetime. However, the old procedure also does not specify a particular conformal transformation of the metric and in effect admits precisely as much freedom. According to the new definition, any two different conformal diagrams of the same spacetime are equivalent in the sense that all the lightrays in those two diagrams will be in an intersection-preserving one-to-one correspondence. In the old language, there must exist a conformal transformation bringing one diagram into the other. Equivalent diagrams carry identical information about the causal structure of the physical spacetime. In the next sections I shall give examples illustrating the arbitrary and the necessary choices involved

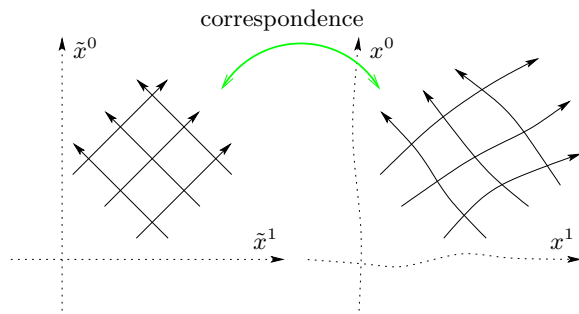


Figure 2: The local correspondence between straight lines drawn at 45° angles in the conformal diagram (left) and light-rays in the physical spacetime (right).

in drawing conformal diagrams.

A conformal diagram delivers information mainly through the shape of its boundary line. The boundary of a conformal diagram generally contains points representing a spacelike, timelike, or null infinity, and points belonging to explicit boundaries of the spacetime manifold (e.g. singularities) where lightrays end in the physical spacetime. The latter boundaries will be called *physical boundaries* to distinguish them from putative *infinite boundaries* whose points do not correspond to any points in the physical spacetime. (The definition of conformal diagrams contains the requirement that the diagram domain be topologically open, and so the boundary points are not supposed to belong to the diagram.) The infinite boundary is of course the most interesting feature of a diagram.

Lastly, I would like to emphasize that conformal diagrams can be drawn not only for geodesically complete spacetimes but also for “artificially incomplete” spacetimes, i.e. for selected subdomains of larger manifolds. In fact such “artificially incomplete” spacetimes are often needed in cosmological applications. Examples are a description of a collapsing star using a subdomain of the Kruskal spacetime and a description of an inflationary universe using a subdomain of the de Sitter spacetime.

2. Minkowski spacetime

The new definition merely lists the conditions to be satisfied by a conformal diagram. Based on these conditions, I shall now develop a practical procedure for drawing the diagrams, using the Minkowski spacetime as the first example.

We begin by choosing a Cauchy surface in the physical spacetime. In 1+1 dimensions, a Cauchy surface is a line L such that intersections of lightrays emitted from L entirely cover the part of the spacetime to the future of L . In the Minkowski spacetime, we may choose the line $x^0 = 0$ as the Cauchy surface L . The image of the Cauchy surface L in the conformal diagram must be a

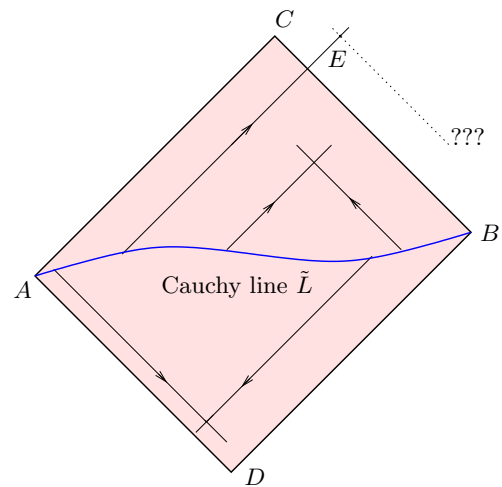


Figure 3: Construction of the conformal diagram for the Minkowski spacetime. The point E cannot belong to the diagram because there are no lightrays intersecting at E .

finite curve \tilde{L} from which lightrays can be emitted in both spatial directions. Therefore the slope of the curve \tilde{L} must not exceed $\pm 45^\circ$ but otherwise \tilde{L} may be drawn arbitrarily, e.g. as the curve AB in Fig. 3. The endpoints A, B represent a spatial infinity in the two directions.

In the Minkowski spacetime, two lightrays emitted towards each other from any two points on L will eventually intersect. Therefore the domain of the conformal diagram must contain at least the triangular region ABC . On the other hand, any point outside ABC , such as the point E in Fig. 3, cannot belong to the diagram domain because the point E cannot be reached by any left-directed lightray emitted from L , and we know that all points in the Minkowski spacetime are intersection points of some lightrays. (More formally, the existence of the point E within the diagram would violate the condition that the correspondence between lightrays is intersection-preserving.) Therefore the future-directed part of the conformal diagram is bounded by the lines AC and BC .

A completely analogous consideration involving past-directed lightrays leads to the conclusion that the past-directed part of the diagram is the region ABD . Thus a possible diagram for the Minkowski spacetime is the interior of the rectangle $ACBD$. This diagram differs from the square-shaped diagram in Fig. 1 by a (finite) conformal transformation of the form (9).

We can also ascertain that the points C and D are the future and the past timelike infinity points. For instance, the point C is the intersection of the lines AC and BC ; these lines are interpreted as putative lightrays emitted from infinitely remote points of L . At sufficiently late times, any inertial observer in the Minkowski spacetime will catch lightrays emitted from arbitrarily far points. The same holds for observers moving non-inertially as long as their velocity does not approach that of light. Hence all trajectories of such observers must finish at C .

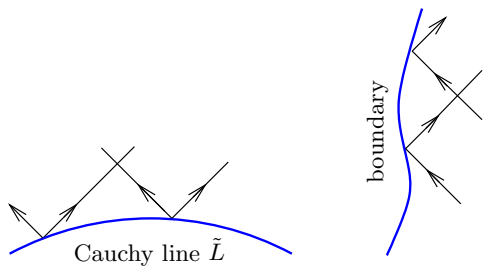


Figure 4: A Cauchy line must have a slope between -45° and 45° (left). A timelike boundary must be a curve with a slope between 45° and 135° (right).

C. Cauchy surfaces and artificial boundaries

Drawing Cauchy surfaces is a convenient starting point in the construction of conformal diagrams.

It is clear that in any 1+1-dimensional spacetime a sufficiently small neighborhood of a Cauchy surface has the same causal properties as the line $x^0 = 0$ in the Minkowski plane: namely, two nearby lightrays emitted toward each other will cross, while rays emitted from a point in opposite directions will diverge. Therefore the line \tilde{L} representing a Cauchy surface in a conformal diagram must have a slope between -45° and 45° (see Fig. 4, left). We shall call such lines *horizontally-directed*. Other than this, there are no restrictions on the shape of the line \tilde{L} and it may be drawn as an arbitrary horizontally-directed curve. (In some spacetimes, one needs to use several disconnected Cauchy surfaces, but I shall not consider such cases here.)

Another frequently occurring feature in conformal diagrams is a *timelike boundary*. For example, a spherically symmetric 3+1-dimensional spacetime is usually reduced to the 1+1-dimensional (r, t) plane, where $0 < r < +\infty$. From the 1+1-dimensional point of view, the line $r = 0$ is an artificially introduced timelike boundary that can absorb and emit lightrays. The local geometry of lightrays near $r = 0$ is shown in Fig. 4 (right). It is clear from the figure that in a conformal diagram the timelike boundary must be represented by a line with a slope between 45° and 135° . We shall call such lines *vertically-directed*.

As an example of using timelike boundaries, let us consider the subdomain $(t_0 < t < \infty, x_1 < x < x_2)$ of a de Sitter spacetime with flat spatial sections, described by the metric

$$g_{ab}dx^a dx^b = dt^2 - e^{2Ht} dx^2. \quad (11)$$

This subdomain can be visualized as the future of a selected initial comoving region. The Cauchy line $t = t_0$ is connected to the two timelike boundary lines, $x = x_{1,2}$. In the coordinate system (11), the null geodesics are solutions of $dx/dt = \pm e^{-Ht}$ and it is easy to see that a lightray emitted at $x = 0, t = 0$ only reaches the values $|x| < H^{-1}$ (the limit value is the de Sitter horizon). Null

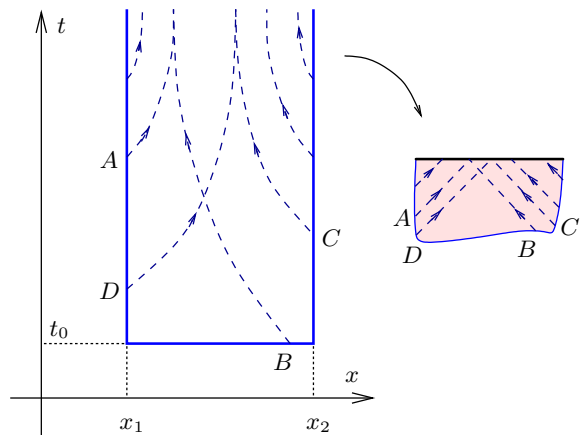


Figure 5: Construction of a conformal diagram for a part of de Sitter spacetime delimited by thick lines (left). The upper boundary of the diagram (right) is a horizontal line.

geodesics emitted from the Cauchy surface and from the boundary lines are sketched in Fig. 5 where it is assumed that the comoving domain $x_1 < x < x_2$ contains several de Sitter horizons. A lightray emitted in the positive direction, such as the ray A , intersects left-directed lightrays emitted from the point B or from nearer points but does not intersect lightrays emitted further away, such as the ray C . We call the ray B the *rightmost ray* intersecting A . It is clear that the intersection of the corresponding lines A and B in the conformal diagram must occur *at the boundary* of the diagram, otherwise there would exist further lines intersecting A to the right of B . Considering a ray D to the right of A , we find that the rightmost ray for D is C . The intersection of C and D is thus another point on the boundary of the conformal diagram. It follows that the boundary line must have a slope between -45° and 45° ; for simplicity, we draw a straight horizontal line (Fig. 5, right). This line represents the (timelike and null) infinite future.

A timelike boundary can be interpreted as the trajectory of an observer who absorbs or emits lightrays and thus participates in the exploration of the causal structure of the spacetime. The lightrays emitted by the boundary, together with those emitted from the Cauchy surface, form the totality of all lightrays that must be bijectively mapped into straight lines in the conformal diagram. The role of timelike boundaries and Cauchy surfaces is to provide a physically motivated boundary for the part of the spacetime we are interested in.

An artificial timelike boundary may also be introduced into the spacetime with the purpose of simplifying the construction of the diagram. Below (Sec. III D) we shall show that conformal diagrams can be pasted together along a common timelike boundary.

D. General procedure

We can now outline a general procedure for building a conformal diagram for a given 1+1-dimensional spacetime using the method of lightrays. The procedure can be applied not only to geodesically complete spacetimes but also to spacetimes with explicitly specified boundaries.

One starts by considering the future-directed part of the spacetime and by choosing a suitable Cauchy surface and, possibly, some timelike boundaries. These lines are represented in the diagram by arbitrarily drawn horizontal and vertical curves of finite extent. The endpoints of these curves correspond either to the intersection points of Cauchy lines and timelike boundaries, or to imaginary points at spacelike and timelike infinity.

Note that Cauchy surfaces and timelike boundaries are the lines on which boundary conditions for e.g. a wave equation must be specified to obtain a unique solution within a domain. One expects that any physically relevant spacetime should contain a suitable set of Cauchy surfaces and timelike boundaries, if the classical field theory is to have predictive power. Qualitative knowledge of the geometry and topology of these boundaries is required for building a conformal diagram using the method of lightrays.

After drawing the curves for the physical boundaries, it remains to determine the shape of the infinite (timelike and null) boundaries of the diagram. To this end, one can first consider *right-directed* lightrays emitted from various points on the Cauchy line and from the boundaries, including the limit points at infinity. For each right-directed lightray X there exists a certain subset \mathcal{S}_X of (left-directed) lightrays that intersect X . Since the subset \mathcal{S}_X has a finite extent, there exists a rightmost ray $r_X \in \mathcal{S}_X$. (In the de Sitter example above, the rightmost ray r_A is the ray B and the rightmost ray r_D is C .) By definition of the conformal diagram, the lightrays are straight lines limited only by the boundary of the conformal diagram, therefore the intersection point of X and r_X must belong to the boundary. In this way we have established the location of one point of the unknown boundary line, namely the endpoint of the ray X .

To determine the local direction of the boundary line at that point, we use the following argument. For each right-directed lightray X , we can consider a right-directed ray X' infinitesimally close and to the right of X (if no ray X' can be found to the right of X , it means that X itself belongs to the boundary of the diagram). Then there are two possibilities (see Fig. 6a,b): either the rightmost ray r_X is also the rightmost ray $r_{X'}$ for X' , or the ray $r_{X'}$ is located to the right of r_X . In the first case, the boundary line has a 45° slope and locally coincides with r_X , while in the second case the boundary line is horizontally-directed. Thus we can draw a right-directed fragment of the infinite boundary that limits the ray X . We then continue by moving further to the right and consider the endpoint of the ray X' , etc.

The same procedure is then repeated for left-directed

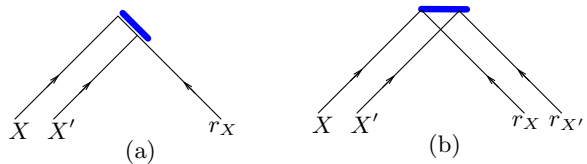


Figure 6: The local direction of the infinite boundary (thick line) is found by determining the rightmost rays $r_X, r_{X'}$ for nearby rays X, X' . The direction is at 45° angle (a) when $r_X = r_{X'}$ and horizontal (b) when $r_X \neq r_{X'}$.

lightrays, until one finishes drawing all unknown lines in the future-directed part of the diagram. In this way the infinite boundary of the conformal diagram is constructed as the locus of “last intersections” of lightrays. Finally one applies the same considerations to past-directed lightrays and so completes the diagram.

It follows that the infinite boundary of a conformal diagram can always be drawn as a sequence of either straight line segments directed at 45° angles, or horizontally- and vertically-directed curves. In our convention, Cauchy surfaces and artificial timelike boundaries are drawn as curved lines and infinite boundaries as straight lines (when possible).

E. Further examples

Collapsing star

The method of lightrays does not require explicit formulae for the spacetime metric if the qualitative behavior of lightrays is known. As another example of using the lightray method, let us consider an asymptotically flat spacetime with a star collapsing to a black hole (BH).

To reduce the spacetime to 1+1 dimensions, we assume spherical symmetry and consider only the (r, t) plane, where $0 < r < +\infty$ and the line $r = 0$, the center of the star, is an artificial boundary. As before, we start with the future-directed part of the diagram. We must first choose a Cauchy surface; a suitable Cauchy surface is the line $t = t_0$ where t_0 is a time chosen before the collapse of the star. We represent the Cauchy surface by the curve AB in the diagram (Fig. 7). The point A corresponds to $(r = 0, t = t_0)$, while B is a spatial infinity $(r = \infty, t = t_0)$. The artificial boundary $r = 0$ is represented by the vertical line AC .

To investigate the shape of the future part of the diagram, we need to analyze the intersections of lightrays emitted from faraway points of the Cauchy surface. We know from qualitative considerations of the black hole formation that lightrays can escape from the star interior only until the appearance of the BH horizon. Shortly thereafter the star center becomes a singularity that cannot emit any lightrays. Hence, among all the rays emitted from the star center at various times, there exists a

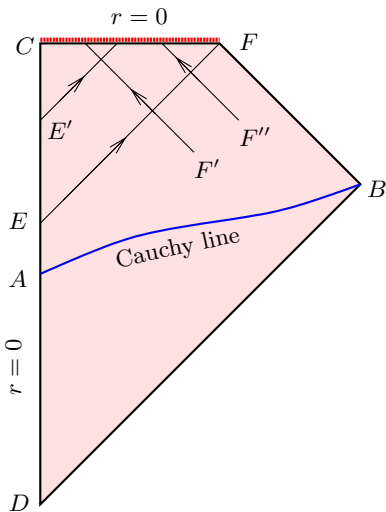


Figure 7: Construction of the conformal diagram for the spacetime of a collapsing star. The thick dotted line CF is a Schwarzschild singularity.

“last ray” not captured by the BH, while rays emitted later are captured. We arbitrarily choose a point E on the boundary line $r = 0$ to represent the emission of this “last ray.” Any lightray emitted from $r = 0$ before E will propagate away from the BH and so will intersect all left-directed lightrays emitted from arbitrarily remote points of the Cauchy line AB . Since all the intersection points are outside of the BH horizon, it follows that the conformal diagram contains the polygon $AEFB$ which represents the spacetime outside the BH. The line FB is the infinite null boundary of the diagram, while the line EF is the BH horizon.

It is clear that the point C is the last point from which lightrays can be emitted from the star center and thus C is the beginning of the BH singularity. It remains to determine the shape of the diagram between the points C and F . We know that a lightray emitted from the center after E will be recaptured by the BH singularity and thus will not intersect with lightrays entering the BH horizon sufficiently late. For instance, the lightray emitted at E' will intersect with the lightray F' but not with a later ray F'' , as shown in Fig. 7. Therefore the diagram boundary line connecting C and F is locally horizontally-directed. This line consists of final intersection points of lightrays emitted from the star center and those entering the BH horizon from outside. These final intersection points are located at the BH singularity which is therefore represented by the entire line CF .

The past-directed part of the conformal diagram is easy to construct. Since any two past-directed lightrays intersect, the past-directed part is similar to that for the Minkowski spacetime with a boundary at $r = 0$, namely the triangular domain ABD . Thus the diagram in Fig. 7 is complete.

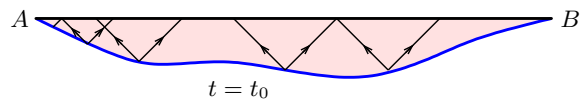


Figure 8: A conformal diagram for the future part of the de Sitter spacetime with flat spatial sections. The curved line represents the spatially infinite Cauchy surface $t = t_0$. The local behavior of lightrays is the same as in Fig. 5.

Future part of de Sitter spacetime

In Fig. 5 we have drawn a conformal diagram for the subdomain of a de Sitter spacetime delimited by two timelike boundaries. We shall now construct the diagram for the future part of a de Sitter spacetime with spatially unlimited sections. (Note that the past half of the de Sitter spacetime is not covered by the flat coordinates because of incompleteness of past-directed geodesics. In this paper we shall not use the complete de Sitter spacetime but only the future of an arbitrarily chosen, unbounded, spacelike Cauchy hypersurface.)

The Cauchy surface $t = t_0$, $-\infty < x < \infty$ is drawn as a finite horizontal curve in the conformal diagram (the curved line AB in Fig. 8). The points A, B in the diagram represent a spacelike infinity in the two directions and do not correspond to any points in the physical spacetime. It remains to establish the shape of the infinite future boundary which must be a line connecting the points A, B to the future of the Cauchy surface. We already know from the construction of the diagram in Fig. 5 that this future boundary is locally horizontal. Since the behavior of lightrays emitted from all points of the Cauchy surface is the same, the future boundary may be represented by a horizontal straight line connecting the points A, B . (To keep the convention of having straight infinite boundaries, we have drawn the Cauchy surface $t = t_0$ as a curve extending downward from the straight line AB .)

Note that the same diagram also represents an inhomogeneous spacetime consisting of de Sitter-like regions with different values of the Hubble constant H . This is so because a difference in the local values of H does not change the qualitative behavior of lightrays at infinity: the rays will intersect only if emitted from sufficiently near points. The infinite future boundary remains a horizontally-directed line as long as $H \neq 0$ everywhere.

The construction of conformal diagrams for the following spacetimes is left as an exercise for the reader.

- A subdomain of the Minkowski spacetime between two causally separated observers moving with a constant proper acceleration in opposite directions (Fig. 9, left).
- A flat closed universe: the subdomain $(-\infty < t < \infty, x_1 < x < x_2)$ of a Minkowski spacetime with the lines $x = x_1$ and $x = x_2$ identified (Fig. 9, right).

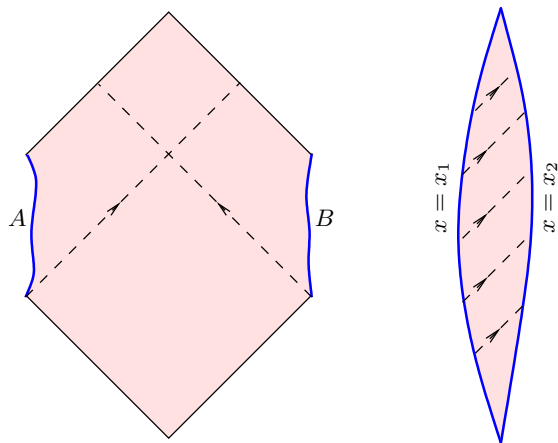


Figure 9: Left: The domain of Minkowski spacetime between two causally separated observers A, B moving with a constant proper acceleration in opposite directions. The dashed lines show that the two observers cannot see each other. Right: A closed Minkowski universe. The thick lines represent the identified boundaries $x = x_{1,2}$. A lightray (dashed line) crosses the line $x = x_{1,2}$ infinitely many times.

- An asymptotically flat spacetime with two stars collapsing into two black holes; the line of sight crosses the two star centers (Fig. 10).
- The future part of a de Sitter spacetime with a star collapsing into a black hole (Fig. 11).
- A maximally extended Schwarzschild-de Sitter spacetime (Fig. 12). It is interesting to note that this diagram is usually drawn with all Schwarzschild and de Sitter regions having the same size, which makes the figure unbounded (Fig. 12, top) despite the intention to represent the spacetime by a *finite* figure in the fiducial Minkowski plane. To adhere to the definition of a conformal diagram as a bounded figure, one can use a suitable conformal transformation reducing the diagram to a finite size (e.g. Fig. 12, bottom).

III. DIAGRAMS FOR ETERNALLY INFLATING SPACETIMES

I now apply the method of lightrays to spacetimes resulting from generic models of eternal inflation. In these models, inflation ends in a particular region of spacetime but continues in nearby regions. The process is analogous to the nucleation of non-inflating bubbles in a de Sitter spacetime. More precisely, the bubble interior inflates at a progressively slower rate until the inflation stops and the interior reheats. In the meantime, the bubble continues to expand, annexing new regions that stop inflating somewhat later. The bubble wall moves with a

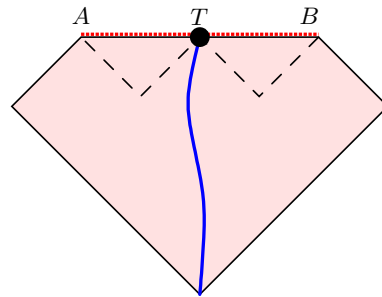


Figure 10: A spacetime with two collapsing stars. The point T is a future timelike infinity reached by an observer (thick curve) remaining between the two black holes. The lines AT and TB represent BH singularities and the dashed lines are the BH horizons.

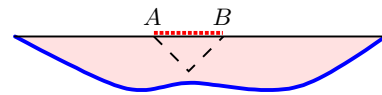


Figure 11: The future part of a de Sitter spacetime with a collapsing star. The line AB represents the BH singularity; the dashed line is the BH horizon.

constant acceleration and its worldline quickly becomes almost lightlike. As was noted in Ref. [11], the interior of the bubble appears to be an infinite FRW universe to an interior observer, even though the bubble occupies a finite interval $x_1 < x < x_2$ of the comoving volume in the background de Sitter spacetime (see Fig. 13). In particular, the hypersurfaces of equal temperature (identified as the equal-time surfaces by interior observers) have an infinite proper volume.

In an eternally inflating spacetime, all Hubble-sized re-

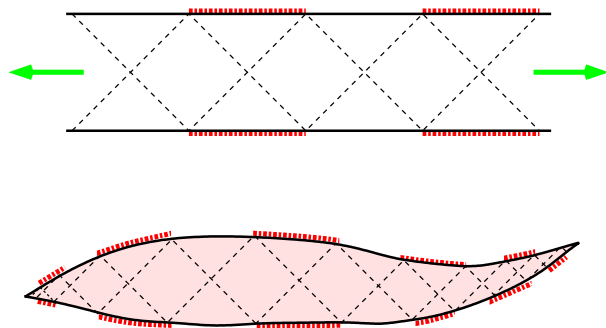


Figure 12: Diagrams for a maximally extended Schwarzschild-de Sitter spacetime. The conventional, unbounded diagram (top) and an equivalent diagram having a finite extent (bottom) are related by a conformal transformation. The thick dotted lines represent Schwarzschild singularities. Both diagrams contain infinitely many Schwarzschild and de Sitter regions.

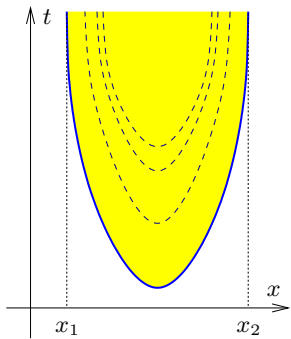


Figure 13: A thermalized bubble in a de Sitter spacetime with flat spatial sections. The dashed lines are equal-temperature surfaces in the thermalized region (shaded).

gions are causally disconnected and thus the nucleation of thermalized bubbles is approximately a Poisson process with a fixed nucleation rate per proper 4-volume. We first construct a conformal diagram for an inflating spacetime with one thermalized bubble and then generalize to a random arrangement of such bubbles. We shall then consider models where the thermalized bubbles eventually become dominated by dark energy and again become patches of the de Sitter spacetime.

A. Spacetime with one bubble

As we have already noted, inflating spacetimes with an inhomogeneous expansion rate are represented by the same conformal diagram as a homogeneous de Sitter spacetime. On the other hand, regions where inflation is finished will have the same causal structure as a flat spacetime. Therefore we can ignore the details of reheating and concentrate on building a conformal diagram for a pure de Sitter spacetime ($H = H_0$) with a nucleating Minkowski bubble ($H = 0$), which is a considerably simpler situation. Since the thickness of bubble walls plays no role in the shape of the resulting conformal diagrams, we shall always treat bubbles in the thin-wall approximation.

We start by choosing a Cauchy surface for the future part of the diagram. An appropriate Cauchy surface would be $t = t_0$ where t_0 is a time moment before the bubble formation. This surface is represented by a spacelike curve in the diagram. We now need to analyze trajectories of lightrays emitted from various points of the Cauchy surface and to determine whether any given pair of lightrays will eventually intersect. As we have seen in Sec. IID, the future infinite boundary of the conformal diagram can be constructed as the locus of “last intersections” of lightrays.

Typical lightray trajectories are sketched in Fig. 14. As in the pure de Sitter spacetime, lightrays not entering the bubble intersect only if emitted from sufficiently

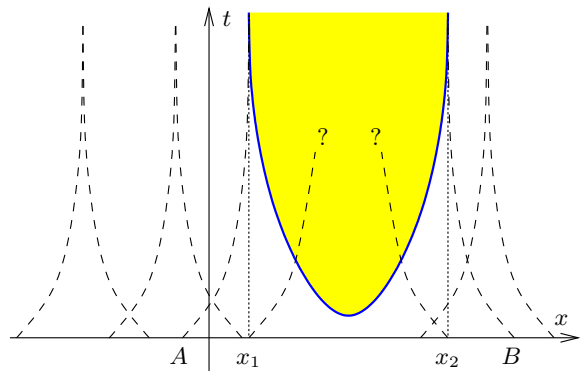


Figure 14: Null geodesics (dashed lines) in a de Sitter spacetime with a bubble (shaded). The last lightrays not entering the bubble are labeled A and B . Question marks indicate that the behavior of lightrays in the bubble interior is yet to be investigated.

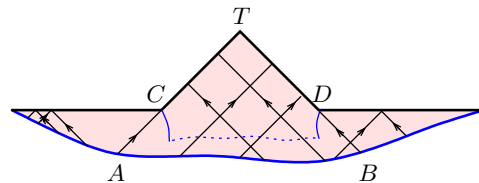


Figure 15: A conformal diagram for the future part of de Sitter spacetime with a dust-dominated bubble. The bubble walls are the vertical curves ending at C and D ; the (spacelike) dotted line symbolizes the nucleation event.

near points. Therefore the rightmost and leftmost lightrays not yet entering the bubble (labeled A, B in Fig. 14) delimit the parts of the conformal diagram that coincide with a pure de Sitter diagram (Fig. 8). Thus the future boundary of our diagram contains two horizontal lines as shown in Fig. 15. The points C, D correspond to the asymptotic comoving positions of the bubble walls ($x = x_{1,2}$).

It remains to determine the behavior of lightrays that do enter the bubble. We shall shortly demonstrate that any two such lightrays necessarily intersect if they enter the bubble from opposite sides. It will then follow that the ray B in Fig. 14 is the rightmost ray for all rays entering the bubble from the left, and likewise the ray A is the leftmost ray for all rays entering from the right. Considerations similar to those used in the construction of the Minkowski diagram (Sec. IIB2) will then show that the infinite boundary of the diagram between the points C and D consists of two null lines CT and TD , while the point T represents a timelike infinity for observers inside the bubble (see Fig. 15).

We shall first give a qualitative argument showing that any two lightrays entering the bubble will eventually intersect. The bubble interior is a certain subdomain of the 1+1-dimensional Minkowski spacetime. Any two light-

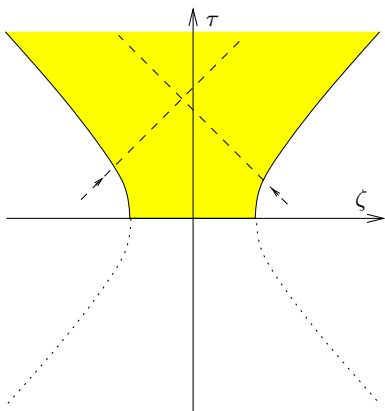


Figure 16: The bubble interior (shaded) viewed in the flat coordinates (τ, ζ) . The dotted lines show the continuation of the bubble wall to times before the bubble nucleation ($\tau = 0$). The dashed lines are lightrays entering the bubble from opposite sides; such lightrays always intersect.

rays entering the bubble from opposite sides will enter the flat subdomain at two spacelike-separated points and will be propagating towards each other. So these rays will eventually intersect somewhere inside the bubble.

To present a more explicit geometric argument, we need to consider the geometry of the bubble interior in some detail. A 1+1-dimensional de Sitter spacetime can be embedded in a flat three-dimensional spacetime with coordinates (τ, w, ζ) and the metric $ds^2 = d\tau^2 - dw^2 - d\zeta^2$ as a hyperboloid

$$\zeta^2 + w^2 - \tau^2 = H_0^{-2} \quad (12)$$

(we follow the notation of Ref. [5]). The geometry of the one-bubble spacetime can be visualized as the union of a part of the de Sitter hyperboloid and a part of a hyperplane $w = w_0$ intersecting the hyperboloid, where $w_0^2 < H_0^{-2}$. The intersection line specified by the equations

$$\zeta^2 - \tau^2 = H_0^{-2} - w_0^2, \quad w = w_0, \quad (13)$$

cuts out the subdomain $\zeta^2 - \tau^2 < H_0^{-2} - w_0^2$ of the Minkowski hyperplane $(\tau, \zeta, w = w_0)$. This subdomain therefore contains the interior of the bubble (Fig. 16). It is then evident that any two opposite lightrays entering the bubble will certainly intersect within its interior. This argument concludes the construction of the conformal diagram shown in Fig. 15.

B. Dark energy-dominated bubble

Let us now consider a cosmological scenario where the thermalized bubble interior eventually becomes dominated by dark energy. If the vacuum energy density is positive then the bubble interior becomes a patch of a de

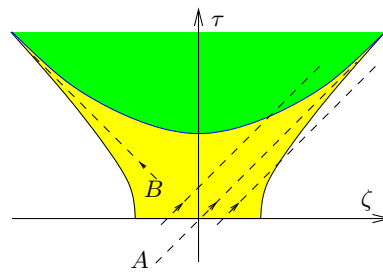


Figure 17: The bubble interior as in Fig. 16 but with a dark energy-dominated subdomain (darker shade). The rays labeled A, B asymptotically coincide with the bubble walls.

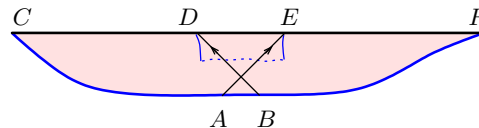


Figure 18: A conformal diagram for the future part of de Sitter spacetime with a dark-energy dominated bubble interior. The bubble walls are shown as in Fig. 15. The points D, E represent the asymptotic position of the bubble walls.

Sitter spacetime. The case of negative dark energy will be considered in the next subsection.

The epoch of dark energy domination begins at an equal-temperature hypersurface at a certain cosmological time t_{DE} after the bubble nucleation. Due to the $SO(3, 1)$ symmetry of the bubble, the dark energy-dominated domain is specified in the flat coordinates (τ, ζ) by the inequality

$$\tau^2 - \zeta^2 > t_{DE}^2, \quad (14)$$

and the boundary $t^2 - \zeta^2 = t_{DE}^2$ approaches the lightcone $\tau = \pm\zeta$ for large τ . It then follows from Fig. 17 that the lightray labeled A separates the right-directed rays exiting the bubble from rays entering and remaining within the dark energy-dominated subdomain. Since the lightray A asymptotically coincides with the bubble wall, the endpoint E of that ray in a conformal diagram (Fig. 18) divides the future infinite boundary CF of the diagram into the parts representing the future of the exterior de Sitter spacetime (EF) and the part corresponding to the interior de Sitter subdomain. Similarly, the ray B divides left-directed rays exiting the bubble from those entering the de Sitter subdomain. The infinite future boundary of the de Sitter subdomain is the same as that in Fig. 8. Therefore a conformal diagram for the spacetime with a dark-energy dominated bubble can be drawn as in Fig. 18 and is the same as the diagram for the future part of a pure de Sitter spacetime. The points D, E are not special with respect to the causal structure and are marked only to specify the asymptotic locations of the bubble walls.

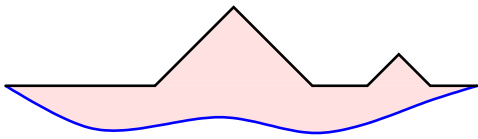


Figure 19: A conformal diagram for the future part of de Sitter spacetime with two dust-dominated bubbles.

C. Bubble dominated by negative dark energy

The last possibility to consider is a bubble that becomes dominated by a negative dark energy (“anti-de Sitter bubble”). This leads to a collapse of the bubble interior into a singularity [11, 12]. Again assuming the $SO(3,1)$ symmetry, we find that the singularity occurs along a spacelike hypersurface $t^2 - \zeta^2 = t_s^2$, where t_s is the cosmological time of collapse. The geometry of the singular surface is quite similar to that of the surface of dark-energy domination, so the singularity may be represented in a conformal diagram by a straight horizontal line connecting the asymptotic positions of the bubble walls. Therefore Fig. 11 may be reused as a conformal diagram for a bubble dominated by negative dark energy if we reinterpret the line AB as a cosmological singularity rather than a Schwarzschild singularity.

D. Many bubbles

Before turning to many-bubble spacetimes, we note that the diagram in Fig. 15 can be obtained by pasting together the diagram in Fig. 5 (right) and the top half of the diagram in Fig. 9 (left). The pasting is performed along the timelike bubble walls treated as artificial boundaries.

Let us briefly consider the pasting of conformal diagrams in general. When two spacetime domains are separated by a timelike worldline, the corresponding conformal diagrams can be pasted together along the boundary line. To verify this almost obvious statement more formally, we begin by drawing the timelike boundary as a vertically-directed line in the diagram. The shape of the conformal diagram to the right of the boundary is determined solely by the intersections of lightrays within the right half of the spacetime. Hence, the conformal diagram for the right half of the spacetime can be pasted to the right of the timelike boundary line. The same holds for the left half of the spacetime. This justifies pasting of diagrams along a common timelike boundary.

It follows that a conformal diagram for a spacetime with *two* nucleating bubbles is a simple concatenation of two diagrams drawn for single-bubble spacetimes. For instance, a diagram for two (nonintersecting) dust-dominated bubbles is shown in Fig. 19. It features two “roofs” representing null and timelike infinities of the two bubble interiors.

Now we consider an eternally inflating spacetime that

contains infinitely many thermalized bubbles at random locations and times. In the comoving coordinates, the walls of each bubble asymptotically approach lines $x = \text{const}$ at late times. We may collect all such lines $x = x_i$, $i = 1, 2, \dots$, into a set $E \equiv \{x_i\}$. This set consists of all comoving trajectories that never enter any thermalized regions. The set E was called the “eternal set” in Ref. [4] where it was shown that E is topologically closed, its comoving measure is zero, and any neighborhood of any point $x_i \in E$ contains infinitely many other points from E (the fractal property). The asymptotic late-time bubble interiors are comoving intervals of x that do not contain any points from E . Infinitely many such intervals cover the entire length of the x axis.

One can visualize the set E as a random Cantor set (see e.g. [13], chapters 8, 23, and 31). A procedure to construct a suitable Cantor set consists of simulating the stochastic process of bubble nucleation (Fig. 20). It is known that bubble intersections are rare in realistic models [14], so we shall for simplicity assume that each bubble expands to the Hubble horizon size in the comoving coordinates. For the purposes of simulation, we can start with an interval $[0, 1]$ of comoving space and divide the time into discrete steps. At each timestep, we randomly choose some bubble nucleation sites using a Poisson process with a fixed number of bubbles per horizon length. At the next step the bubbles grow to horizon size, so the corresponding segments are removed from the interval and new nucleation sites are chosen. The horizon size decreases geometrically with time and thus the number of removed intervals grows and their length decreases. The set E consists of points that have not been removed after infinitely many steps (computer time permitting).

In the conformal diagram, the infinite future of each bubble interior is represented by a “roof” if the bubble is dust-dominated and by a horizontal line if the bubble is dark energy-dominated. Since the latter case results in a rather uninteresting diagram (the same as in Fig. 18 but with infinitely many bubble walls), we shall confine our attention to dust-dominated bubbles. A conformal diagram for that case is shown in Fig. 21 and can be constructed as follows. First we imagine a pure de Sitter region without bubbles and draw its infinite future boundary (dashed line in Fig. 21). Then the asymptotic positions of bubble walls are marked on that line as the points of a random Cantor set E . Finally, each interval not containing any points from E is raised to a “roof” representing a null and a timelike infinity of the bubble interior.

It follows from the fractal property of the set E that there exist infinitely many arbitrarily small roofs between any two roofs in Fig. 21. Thus a conformal diagram for an eternally inflating spacetime must contain a fractal arrangement of infinitely many lines.

I conclude this section by a comment on the relevance of 1+1-dimensional diagrams to 3+1-dimensional universes. As I have noted above, the reduction to a 1+1-dimensional slice is useful only if all null geodesics

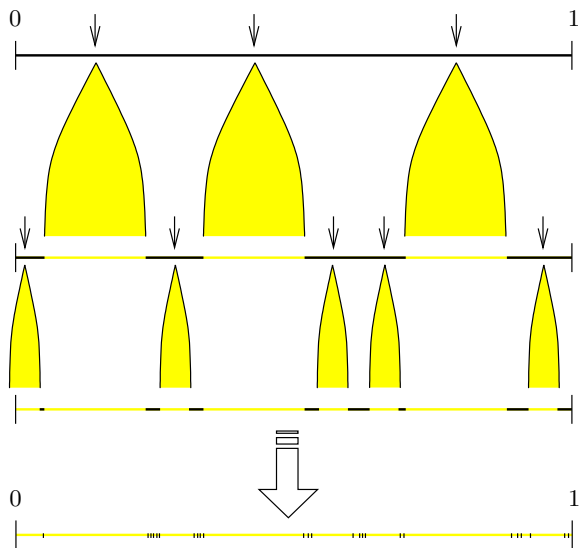


Figure 20: Construction of a random Cantor set. Arrows show the bubble nucleation sites randomly chosen at each timestep. The (comoving) bubble size decreases geometrically with time and the number of nucleation sites increases. After infinitely many steps, there remains a fractal set of points (sketched below).

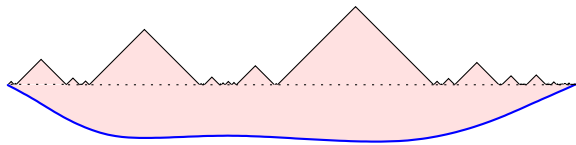


Figure 21: A conformal diagram for the future part of an eternally inflating spacetime with a fractal arrangement of dust-dominated bubbles. (A computer simulation was used to position the bubbles.)

within the slice are also geodesics in the full spacetime. This is the case for a spherically symmetric spacetime reduced to the (t, r) slice, but generally not for a (t, x) slice of a (t, x, y, z) spacetime with a random distribution of bubbles, even if each bubble were spherically symmetric. However, we are presently considering an inflationary spacetime with a geometry that is approximately de Sitter in large (super-Hubble) domains. Then one can define the local expansion rate $H(t, x, y, z)$ which is a slowly-changing function in both space and time. In this case the null lines within an arbitrary 1+1-dimensional slice, such as the slice (t, x) , are approximately geodesic lines in the full spacetime. Therefore the diagram in Fig. 21 can be used as a qualitative visualization of the causal structure of such a spacetime along a randomly chosen line of sight.

IV. DIAGRAMS FOR RECYCLING UNIVERSES

In quantum field theory there exist several possibilities for a transition, via bubble nucleation, from one de Sitter (dS) state to another dS state having a different vacuum energy [11, 15, 16]. The model of a recycling universe [5] involves such “false-vacuum bubbles” randomly nucleating in regions of true vacuum. Within the nucleated dS bubbles, inflation begins anew (“recycling”) and eventually creates new thermalized regions of true vacuum. The process of recycling repeats *ad infinitum*. Note that the geometry resulting from the nucleation of false-vacuum bubbles is qualitatively different from that resulting from a cosmological dark-energy domination, because the latter occurs everywhere in the bubble interior, while nucleated bubbles typically never merge to fill the entire spatial volume [14].

The model of the string theory landscape [6] is a general cosmological scenario where locally de Sitter-like regions can randomly nucleate asymptotically flat (“Minkowski”), de Sitter, or “anti-de Sitter” (AdS) bubbles. The dS bubbles can nucleate further bubbles in their interior and thus give rise to the recycling process. On the other hand, AdS regions (more precisely, bubbles that are eventually dominated by a negative dark energy) will collapse to a singularity. So we assume that no further bubbles can be nucleated within AdS or Minkowski bubbles.

In this last section we consider cosmological scenarios involving the phenomenon of recycling and draw the corresponding conformal diagrams.

We begin by building a conformal diagram for a flat spacetime with one nucleated dS bubble (although this process does not happen spontaneously, the diagram is still useful). It is convenient to choose a spherically symmetric slice (t, r) with an artificial boundary $r = 0$, and a Cauchy surface preceding the bubble nucleation. Then the past-directed part of the diagram is the same as for the Minkowski spacetime, so we concentrate on the future part.

The geometry of spherically symmetric false-vacuum bubbles embedded in Minkowski regions is lucidly presented in Ref. [17] and I shall merely outline the results here. The bubble wall is moving with a constant acceleration towards the region of higher expansion rate H . At a certain time, the bubble wall implodes upon itself and disappears from view under a Schwarzschild horizon. From that time onwards, the bubble appears to be a black hole when viewed from outside. The corresponding part of the diagram is similar to that in Fig. 7, and thus we can start drawing Fig. 22. However, as explained in Ref. [17] and illustrated in Figs. 12-13 therein, the part of the spacetime not accessible to exterior observers has a more complicated structure than a usual BH interior. In fact this part of the spacetime contains a spatially closed, causally disconnected universe which I shall call the “interior universe” for brevity. The interior universe contains subdomains of Schwarzschild and of de Sitter (dS) space-

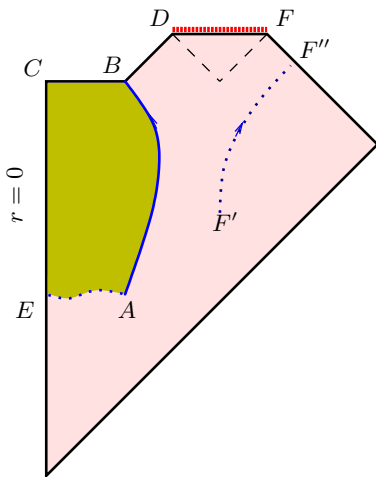


Figure 22: A flat spacetime with a nucleated de Sitter bubble. The bubble appears as a black hole from outside (cf. Fig. 7) but contains a de Sitter patch in its interior (shaded). The line AB is the bubble wall, EA is the nucleation surface, DF is the BH singularity, BC is the de Sitter asymptotic future, and the dashed line is the BH horizon. The line $F'F''$ is a trajectory accelerating away from the BH.

time. The bubble wall does not collapse onto the BH singularity but passes into the interior universe where it continues to expand with a constant acceleration, away from the inner Schwarzschild horizon. Beyond the bubble wall there is an expanding subdomain of a de Sitter spacetime.

The bubble wall is a timelike boundary that allows us to combine the partial de Sitter diagram for the bubble interior (Fig. 5, right) with a diagram for the rest of the interior universe. To obtain the latter, we forget about the bubble for a moment and consider a trajectory of an observer uniformly accelerating away from a Schwarzschild horizon. This is the line $F'F''$ in Fig. 22 where we have used the exterior Schwarzschild horizon as an illustration. The range FF'' of the boundary line is the null future for rays that escape from the BH but cannot overtake the accelerated observer. A similar configuration occurs in the interior universe where the bubble wall accelerates away from the inner BH horizon. Thus in the interior universe there must exist lightrays escaping the inner BH horizon but never overtaking the bubble wall. The null future of such lightrays is a line at 45° angle (the line BD in Fig. 22) connecting the BH singularity (DF) with the asymptotic future of the bubble wall (point B).

This argument concludes the justification of the diagram in Fig. 22 which is equivalent to the appropriate part of Fig. 15 in Ref. [17].

More realistically, we can consider high- H bubbles nucleating within low- H de Sitter regions. There are two qualitatively different cases: the nucleated bubble may have either subhorizon or superhorizon size in the back-

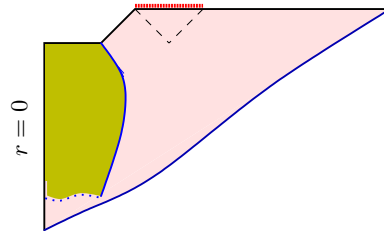


Figure 23: A future part of the dS spacetime with a dS bubble having a higher expansion rate (cf. Fig. 22). The initial radius of the bubble is assumed to be smaller than the background dS horizon.

ground dS spacetime. In the present paper I shall not be concerned with the relative likelihood of these processes but simply consider both cases. Since there is an unbounded 4-volume in which to nucleate bubbles, all possible nucleation processes will occur infinitely many times, no matter how small the nucleation rate.

If the nucleated bubble is smaller than the background horizon, the wall will implode and form a black hole quite similarly to the situation in the Minkowski background. The corresponding diagram, Fig. 23, is different from Fig. 22 only in the parts relevant to the exterior universe which is now de Sitter rather than Minkowski (cf. Fig. 11 for the relevant part of the Schwarzschild-de Sitter diagram).

If the nucleated bubble has super-horizon size, the wall will not collapse but will asymptotically approach the horizon size, moving inwards. The diagram for this case is that shown in Fig. 18.

Finally, a dust-dominated bubble in a de Sitter background can further nucleate a nested de Sitter bubble. A diagram for such a spacetime is Fig. 24, where we have shown both sides of the bubbles rather than only one side as in Figs. 23 and 22.

Using all possible nested nucleations as building blocks, we can now sketch a diagram for a “recycling landscape” featuring a stochastic arrangement of dS, AdS, and dust-dominated bubbles nucleated randomly within each other (Fig. 25). The infinite future boundary of the conformal diagram is a fractal line whose fragments are taken from the diagrams in Figs. 11, 15, 18, 21, 22, 23, and 24. Of course, a drawing printed on paper cannot represent the entire structure of a fractal line. In reality, there are (almost surely) infinitely many nucleated bubbles between any two such bubbles.

This diagram concludes the present investigation of the causal structure of eternally inflating spacetimes.

Acknowledgments

The author is grateful to Slava Mukhanov, Matthew Parry, Sergei Solodukhin, and Alex Vilenkin for stimulating discussions, and to Jaume Garriga and Alex Vikman

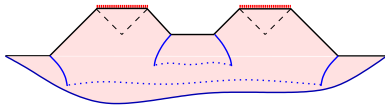


Figure 24: A future part of the dS spacetime with a nucleated dust-dominated bubble and a nested dS bubble (cf. Fig. 23). The black hole horizons, bubble walls, and nucleation surfaces are shown as in Figs. 15 and 22.

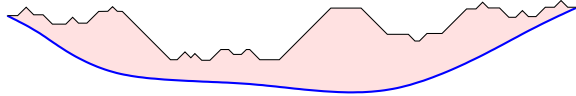


Figure 25: A sketch of a diagram for the future part of a recycling dS spacetime, featuring a random arrangement of nested bubbles of all types. Schwarzschild singularities are not shown.

for useful comments on the manuscript.

-
- [1] A. Vilenkin, Phys. Rev. D **27**, 2848 (1983).
 [2] A. D. Linde, Phys. Lett. B **175**, 395 (1986).
 [3] M. Aryal and A. Vilenkin, Phys. Lett. B **199**, 351 (1987).
 [4] S. Winitzki, Phys. Rev. D **65**, 083506 (2002) [gr-qc/0111048].
 [5] J. Garriga and A. Vilenkin, Phys. Rev. D **57**, 2230 (1998) [astro-ph/9707292].
 [6] L. Susskind, “The anthropic landscape of string theory” [preprint hep-th/0302219].
 [7] G. ’t Hooft, in *Salanfestschrift*, p. 284, ed. by A. Alo, J. Ellis, and S. Randjibar-Daemi, World Scientific, Singapore, 1993 [gr-qc/9310006].
 [8] L. Susskind, J. Math. Phys. **36**, 6377 (1995) [hep-th/9409089].
 [9] R. Bousso, Class. Quant. Grav. **17**, 997 (2000) [hep-th/9911002]; Rev. Mod. Phys. **74**, 825 (2002) [hep-th/0203101].
 [10] N. D. Birrell and P. C. W. Davies, *Quantum fields in curved space* (Cambridge University Press, 1982).
 [11] S. Coleman and F. De Luccia, Phys. Rev. D **21**, 3305 (1980).
 [12] L. F. Abbott and S. Coleman, Nucl. Phys. B **259**, 170 (1985).
 [13] B. Mandelbrot, *The fractal geometry of nature* (Freeman, New York, 1983).
 [14] A. H. Guth and E. J. Weinberg, Nucl. Phys. B **212**, 321 (1983).
 [15] K. Lee and E. J. Weinberg, Phys. Rev. D **36**, 1088 (1987).
 [16] J. Garriga and A. Megevand, Int. J. Theor. Phys. **43**, 883 (2004) [hep-th/0404097].
 [17] S. K. Blau, E. I. Guendelman, and A. H. Guth, Phys. Rev. D **35**, 1747 (1987).